arXiv:1406.5256v2 [hep-ph] 16 Jul 2014

Precision calculations for the T-odd quark pair production at the CLIC e^+e^- linear collider

A. B. Mahfoudh, Guo Lei, Liu Wen, Ma Wen-Gan, Zhang Ren-You, and Zhang Wen-Juan
Department of Modern Physics, University of Science and Technology of China (USTC),
Hefei, Anhui 230026, P.R.China

Abstract

We perform the precision calculations for the $e^+e^- \to q_-\bar{q}_-$ ($q_-\bar{q}_- = u_-\bar{u}_-,\ c_-\bar{c}_-,\ d_-\bar{d}_-,\ s_-\bar{s}_-$) processes up to the QCD next-to-leading order (NLO) including full weak decays for the final T-odd mirror quarks in the littlest Higgs model with T-parity (LHT) at the Compact Linear Collider (CLIC). We show the dependence of the leading order (LO) and NLO QCD corrected cross sections on the colliding energy $\sqrt{s}$, and provide the LO and QCD NLO kinematic distributions of final particles. The results show that the LO cross section can be enhanced by the NLO QCD correction and the K-factor increases obviously when the threshold of the on-shell $q_-\bar{q}_-$-pair production approaches the colliding energy $\sqrt{s}$. The K-factor value varies in the range of $1.04 \sim 1.41$ in our chosen parameter space. We find that a simple approximation of multiplying the LO kinematic distribution with the integrated K-factor is not appropriate for precision study of the $e^+e^- \to q_-\bar{q}_-$ ($q_-\bar{q}_- = u_-\bar{u}_-,\ c_-\bar{c}_-,\ d_-\bar{d}_-,\ s_-\bar{s}_-$) processes, since the NLO QCD corrections are phase space dependent. It is necessary to calculate the differential cross sections including full NLO QCD corrections to get reliable results.

PACS: 12.38.Bx, 13.85.Dz, 13.66.Hk

Keywords: Littlest Higgs model with T-parity, Compact Linear Collider, NLO QCD

I. Introduction

The Compact Linear Collider (CLIC) is a high-luminosity TeV scale e^+e^- linear collider under development. It is schemed that CLIC would provide high luminosity e^+e^- collisions from a few hundred GeV to 3 TeV. The first stage of CLIC, with energy at or above 350 GeV, gives access to precision Higgs physics, providing absolute values of Higgs couplings to both fermions and bosons. This stage also addresses precision top physics. The second stage, around 1.4 TeV, will open the energy frontier allowing for the discovery of new physics phenomena. The ultimate CLIC energy would be 3 TeV which enlarges the CLIC physics potential even further [1]. Therefore, this machine is considered an important option for a post-LHC facility at CERN, as emphasized in the recent update of the european strategy for particle physics [2, 3]. Due to the cleaner environment arising from e^+e^- collisions and the compelling high energy, the CLIC could produce new heavy particles with exciting precision, and can be expected to provide more significant information about new physics.

The Higgs boson discovery reported by the CERN Large Hadron Collider (LHC) experiments [4,5] indeed strengthens our confidence in the standard model (SM) [6–15] which has made remarkable success in accurately describing particle physics including the strong and electroweak interactions. However, the notorious hierarchy problem which describes the unstable mass of Higgs from the SM under radiative corrections exists in the framework of the SM. By introducing a set of new heavy gauge bosons (W_H, Z_H, A_H), a vector-like quark (T) and a Higgs triplet (Φ) at the global symmetry breaking scale f, the littlest Higgs (LH) model could cancel the quadratic divergences of the Higgs mass at one-loop level [16]. Nevertheless, the LH model suffers severe constraints from precision electroweak measurements. The littlest Higgs model with T-parity (LHT) could solve this problem successfully by bringing in a Z_2 discrete symmetry described as T-parity, and can avoid fine-tuning between the global symmetry breaking scale f and the electroweak symmetry breaking scale [17–20]. Furthermore, the LHT could offer a candidate for dark matter [18–22]. Thus we should pay more attention to the LHT. Recently, some QCD next-to-leading order (NLO) phenomenological aspects of the LHT have been analyzed in Refs. [23–25].

In this work, we study the $q_-\bar{q}_-$-pair production up to the QCD NLO in the LHT at the e^+e^- CLIC including subsequential decays of the final T-odd quarks. We organize this paper as follows: In

Sec.II, we describe the related LHT theory, and provide the NLO QCD corrected decay widths of the T-odd quarks. In Sec.III, the calculation strategy is presented. In Sec.IV, numerical analysis and a discussion are provided. A short summary is given finally.

II. Related LHT theory

In the LHT scenario, 14 massless Nambu-Goldstone bosons are born out of an $SU(5)$ global symmetry breaking down to $SO(5)$ spontaneously at some high-scale f. Four of them are regarded as longitudinal modes of the heavy gauge bosons. The other 10 decompose into a T-even SU(2) doublet h, treated as the SM Higgs doublet, and a complex T-odd $SU(2)$ triplet Φ. To implement T-parity in the fermion sector of the model, the mirror partners for each of the original fermions are introduced. The masses of the T-odd partners of SM up- and down-type quarks are expressed as

$$m_{u_-}, m_{c_-} \simeq \sqrt{2}\kappa f\left(1-\frac{1}{8}\frac{v^2}{f^2}\right), \qquad m_{d_-}, m_{s_-} = \sqrt{2}\kappa f, \tag{2.1}$$

where κ is the mass coefficient in Lagrangian of the quark sector, and the vacuum expectation value $v = 246$ GeV. The masses of the T-odd gauge bosons are given by

$$m_{A_H} \simeq \frac{1}{\sqrt{5}} g' f\left(1-\frac{5}{8}\frac{v^2}{f^2}\right), \quad m_{W_H} \simeq gf\left(1-\frac{1}{8}\frac{v^2}{f^2}\right), \quad m_{Z_H} \simeq m_{W_H}. \tag{2.2}$$

The Feynman rules for the vertices in the LHT related to this work are listed in Table 1, where $\delta_v = -\frac{v^2}{8f^2}$, $P_{L,R} = \frac{1}{2}(1 \mp \gamma_5)$ and θ_W is the Weinberg angle. The details of the LHT theory can be found in Refs. [18–20, 26, 27].

Interaction	Feynman rule	Interaction	Feynman rule
$\bar{U}_{i-} Z^\mu U_{i-}$	$\frac{ig}{\cos\theta_W}\left(\frac{1}{2} - \frac{2}{3}\sin^2\theta_W + \delta_v P_L\right)\gamma^\mu$	$\bar{D}_{i-} Z^\mu D_{i-}$	$\frac{ig}{\cos\theta_W}\left(-\frac{1}{2} + \frac{1}{3}\sin^2\theta_W\right)\gamma^\mu$
$\bar{U}_{i-} A^\mu U_{i-}$	$ieQ_{U_{i-}}\gamma^\mu$	$\bar{D}_{i-} A^\mu D_{i-}$	$ieQ_{D_{i-}}\gamma^\mu$
$\bar{U}_{i-} A_H^\mu U_j$	$i\left(-\frac{g'}{10}\cos\theta_H - \frac{g}{2}\sin\theta_H\right)(V_{Hu})_{ij}\gamma^\mu P_L$	$\bar{D}_{i-} A_H^\mu D_j$	$i\left(-\frac{g'}{10}\cos\theta_H + \frac{g}{2}\sin\theta_H\right)(V_{Hd})_{ij}\gamma^\mu P_L$
$\bar{U}_{i-} Z_H^\mu U_j$	$i\left(-\frac{g'}{10}\sin\theta_H + \frac{g}{2}\cos\theta_H\right)(V_{Hu})_{ij}\gamma^\mu P_L$	$\bar{D}_{i-} Z_H^\mu D_j$	$i\left(-\frac{g'}{10}\sin\theta_H - \frac{g}{2}\cos\theta_H\right)(V_{Hd})_{ij}\gamma^\mu P_L$
$\bar{D}_{i-} W_H^{-\mu} U_j$	$i\frac{g}{\sqrt{2}}(V_{Hu})_{ij}\gamma^\mu P_L$	$\bar{U}_{i-} W_H^{+\mu} D_j$	$i\frac{g}{\sqrt{2}}(V_{Hd})_{ij}\gamma^\mu P_L$
$\bar{q}_-^\alpha q_-^\beta G_\mu^a$	$ig_s(T^a)_{\alpha\beta}\gamma^\mu$		

Table 1: The related LHT Feynman rules used in this work, where $U_{i-} = u_-, c_-$ and $D_{i-} = d_-, s_-$, $i, j = 1, 2$ are the generation indices.

The LO partial decay widths of T-odd up- and down-type mirror quarks can be found in Appendix B of Ref. [24]. We calculate the NLO QCD corrected partial decay widths of T-odd up- and down-type mirror quarks of the first two generations in case of neglecting light quark masses and the terms of order $(\alpha_s/\pi)m^2_{V_H}/m^2_{q_-}$ ($V_H = Z_H, W_H, A_H$), which can be accepted in the parameter space adopted in this work. The explicit expressions for the relevant partial decay widths at NLO can be written as

$$
\begin{aligned}
\Gamma(U_{i-} \to A_H U_j) &= \frac{2|(V_{Hu})_{ij}|^2 \left(\frac{g s_H}{2} + \frac{g' c_H}{10}\right)^2}{64\pi} \frac{m^3_{U_{i-}}}{m^2_{A_H}} \left(1 - \frac{m^2_{A_H}}{m^2_{U_{i-}}}\right)^2 \left(1 + \frac{2m^2_{A_H}}{m^2_{U_{i-}}}\right) \\
&\quad \left[1 - \frac{2\alpha_s}{3\pi}\left(\frac{2\pi^2}{3} - \frac{5}{2}\right)\right], \qquad (i,j = 1,2), \\
\Gamma(U_{i-} \to Z_H U_j) &= \frac{2|(V_{Hu})_{ij}|^2 \left(\frac{g c_H}{2} - \frac{g' s_H}{10}\right)^2}{64\pi} \frac{m^3_{U_{i-}}}{m^2_{Z_H}} \left(1 - \frac{m^2_{Z_H}}{m^2_{U_{i-}}}\right)^2 \left(1 + \frac{2m^2_{Z_H}}{m^2_{U_{i-}}}\right) \\
&\quad \left[1 - \frac{2\alpha_s}{3\pi}\left(\frac{2\pi^2}{3} - \frac{5}{2}\right)\right], \qquad (i,j = 1,2), \\
\Gamma(U_{i-} \to W^+_H D_j) &= \frac{g^2|(V_{Hd})_{ij}|^2}{64\pi} \frac{m^3_{U_{i-}}}{m^2_{W_H}} \left(1 - \frac{m^2_{W_H}}{m^2_{U_{i-}}}\right)^2 \left(1 + \frac{2m^2_{W_H}}{m^2_{U_{i-}}}\right) \\
&\quad \left[1 - \frac{2\alpha_s}{3\pi}\left(\frac{2\pi^2}{3} - \frac{5}{2}\right)\right], \qquad (i,j = 1,2), \\
\Gamma(D_{i-} \to A_H D_j) &= \frac{2|(V_{Hd})_{ij}|^2 \left(\frac{g s_H}{2} - \frac{g' c_H}{10}\right)^2}{64\pi} \frac{m^3_{D_{i-}}}{m^2_{A_H}} \left(1 - \frac{m^2_{A_H}}{m^2_{D_{i-}}}\right)^2 \left(1 + \frac{2m^2_{A_H}}{m^2_{D_{i-}}}\right) \\
&\quad \left[1 - \frac{2\alpha_s}{3\pi}\left(\frac{2\pi^2}{3} - \frac{5}{2}\right)\right] \qquad (i,j = 1,2), \\
\Gamma(D_{i-} \to Z_H D_j) &= \frac{2|(V_{Hd})_{ij}|^2 \left(\frac{g c_H}{2} + \frac{g' s_H}{10}\right)^2}{64\pi} \frac{m^3_{D_{i-}}}{m^2_{Z_H}} \left(1 - \frac{m^2_{Z_H}}{m^2_{D_{i-}}}\right)^2 \left(1 + \frac{2m^2_{Z_H}}{m^2_{D_{i-}}}\right) \\
&\quad \left[1 - \frac{2\alpha_s}{3\pi}\left(\frac{2\pi^2}{3} - \frac{5}{2}\right)\right] \qquad (i,j = 1,2), \\
\Gamma(D_{i-} \to W^-_H U_j) &= \frac{g^2|(V_{Hu})_{ij}|^2}{64\pi} \frac{m^3_{D_{i-}}}{m^2_{W_H}} \left(1 - \frac{m^2_{W_H}}{m^2_{D_{i-}}}\right)^2 \left(1 + \frac{2m^2_{W_H}}{m^2_{D_{i-}}}\right) \\
&\quad \left[1 - \frac{2\alpha_s}{3\pi}\left(\frac{2\pi^2}{3} - \frac{5}{2}\right)\right] \qquad (i,j = 1,2),
\end{aligned}
\tag{2.3}
$$

where $U_{i-} = u_-, c_-$, $D_{i-} = d_-, s_-$, $U_i = u, c$, $D_i = d, s$, $s_H = \sin\theta_H$, $c_H = \cos\theta_H$, and the mixing angle θ_H at the $\mathcal{O}(v^2/f^2)$ is expressed as

$$
\sin\theta_H \simeq \left[\frac{5gg'}{4(5g^2 - g'^2)} \frac{v^2}{f^2}\right]. \tag{2.4}
$$

As discussed in Ref. [28], the two mixing matrices satisfy $V^\dagger_{Hu} V_{Hd} = V_{CKM}$. Therefore, they cannot

simultaneously be set to the identity. In the following calculations we take V_{Hu} to be a unit matrix, then we have $V_{Hd} = V_{CKM}$. The NLO QCD corrected total decay width of the T-odd quark q_- can be obtained approximately by summing up all the NLO partial decay widths of the main decay channels shown in Eqs.(2.3).

III. Calculations

We employ the FeynArts 3.4 package [29] to generate Feynman diagrams and their corresponding amplitudes in the LO and QCD NLO calculations. The t'Hooft-Feynman gauge is adopted in this work except when we verify the gauge invariance. The reduction of the amplitudes are implemented by the FormCalc 5.4 programs [30].

III..1 LO cross section

The contribution to the cross section of process $e^+e^- \to q_-\bar{q}_-$ in the LHT at the lowest order is of $\mathcal{O}(\alpha_{ew}^2)$ with pure electroweak interactions. We present the tree-level Feynman diagrams in Fig.1. The $e^+e^- \to q_-\bar{q}_-$ process at the CLIC can be denoted as

$$e^+(p_1) + e^-(p_2) \to q_-(p_3) + \bar{q}_-(p_4), \qquad (q_-\bar{q}_- = u_-\bar{u}_-, c_-\bar{c}_-, d_-\bar{d}_-, s_-\bar{s}_-) \tag{3.1}$$

where p_i $(i = 1, 2, 3, 4)$ represent the four-momenta of the incoming and outgoing particles. The differential cross section for the process $e^+e^- \to q_-\bar{q}_-$ at the tree-level with unpolarized incoming particles can be obtained as

$$d\sigma^0_{q_-\bar{q}_-} = \frac{1}{4}\frac{(2\pi)^4 N_c}{4|\vec{p}_1|\sqrt{s}} \sum_{spin} |\mathcal{M}^0_{q_-\bar{q}_-}|^2 d\Phi_2, \tag{3.2}$$

where the color number $N_c = 3$ and the summation is taken over the spins of initial and final particles. The factor $\frac{1}{4}$ is due to taking average over the polarization states of the electron and positron. $d\Phi_2$ is the two particle phase space element defined as

$$d\Phi_2 = \delta^{(4)}\left(p_1 + p_2 - p_3 - p_4\right) \prod_{i=3}^{4} \frac{d^3\vec{p}_i}{(2\pi)^3 2E_i}. \tag{3.3}$$

In this work we provide the total cross section and distributions for all the $(u_-\bar{u}_-), (c_-\bar{c}_-), (d_-\bar{d}_-), (s_-\bar{s}_-)$ pair production processes. The LO total cross section for processes (3.1) can be figured out from the

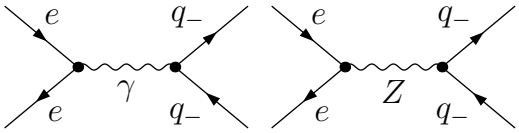

Figure 1: The lowest order Feynman diagrams for the $e^+e^- \to q_-\bar{q}_-$ process in the LHT.

following formula:

$$\sigma_{LO} = \sum_{q_-=u_-,d_-,c_-,s_-} \sigma^0_{q_-\bar{q}_-}. \tag{3.4}$$

III..2 QCD NLO corrections to $e^+e^- \to q_-\bar{q}_-$ process

The QCD NLO corrections to the process $e^+e^- \to q_-\bar{q}_-$ at the CLIC can be divided into two parts: (i) The QCD one-loop virtual corrections to the processes $e^+e^- \to q_-\bar{q}_-$; (ii) The contributions of the real gluon emission process $e^+e^- \to q_-\bar{q}_-g$. In the NLO calculations we adopt the dimensional regularization scheme, in which the dimensions of spinor and space-time manifolds are extended to $D = 4-2\epsilon$ to isolate the ultraviolet (UV) and infrared (IR) singularities. The representative Feynman diagrams for the one-loop virtual corrections to the process $e^+e^- \to q_-\bar{q}_-$ are presented in Fig.2. There exist both UV and IR singularities. The masses and wave functions of T-odd partners of SM quarks should be renormalized to remove the UV divergences. The counterterms are defined as

$$\begin{aligned} \psi^{0,L,R}_{q_-} &= \left(1+\frac{1}{2}\delta Z^{L,R}_{q_-}\right)\psi^{L,R}_{q_-}\,, \\ m^0_{q_-} &= m_{q_-}+\delta m_{q_-}\,, \end{aligned} \tag{3.5}$$

where $\psi^{L,R}_{q_-}$ denote the fields of T-odd mirror quark, and m_{q_-}denotes the mass of T-odd mirror quark. Taking the on-mass-shell renormalized condition we get the renormalization constants as

$$\begin{aligned} \delta Z^{L,R}_{q_-} &= -\frac{\alpha_s(\mu_r)}{3\pi}\left[\Delta_{UV}+2\Delta_{IR}+4+3\ln\left(\frac{\mu_r^2}{m^2_{q_-}}\right)\right]\,, \\ \frac{\delta m_{q_-}}{m_{q_-}} &= -\frac{\alpha_s(\mu_r)}{3\pi}\left\{3\left[\Delta_{UV}+\ln\left(\frac{\mu_r^2}{m^2_{q_-}}\right)\right]+4\right\}\,. \end{aligned} \tag{3.6}$$

There $\Delta_{UV} = \frac{1}{\epsilon_{UV}} - \gamma_E + \ln(4\pi)$ and $\Delta_{IR} = \frac{1}{\epsilon_{IR}} - \gamma_E + \ln(4\pi)$. The one-loop virtual contribution is UV finite after performing the renormalization procedure. The remaining IR divergencies can be

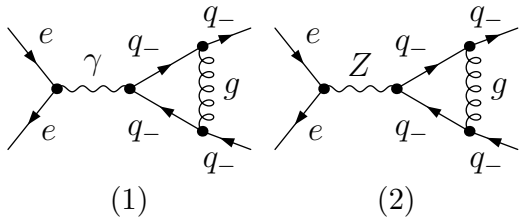

Figure 2: The representative one-loop Feynman diagrams for the process $e^+e^- \to q_-\bar{q}_-$.

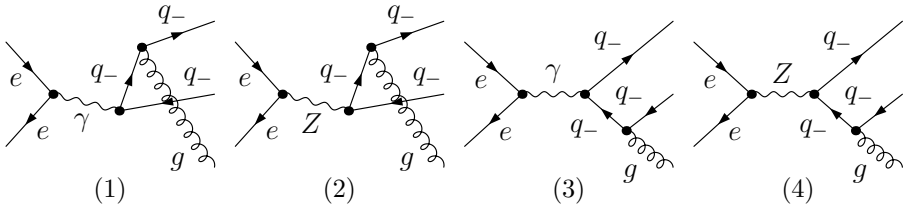

Figure 3: The tree-level Feynman diagrams for the real gluon emission process $e^+e^- \to q_-\bar{q}_-g$.

cancelled by the real gluon bremsstrahlung corrections in the soft gluon limit, as we shall see later.

The real gluon emission process is denoted as

$$e^+(p_1) + e^-(p_2) \to q_-(p_3) + \bar{q}_-(p_4) + g(p_5), \qquad (q_-\bar{q}_- = u_-\bar{u}_-, c_-\bar{c}_-, d_-\bar{d}_-, s_-\bar{s}_-), \tag{3.7}$$

where the real gluon radiates from $q_-(\bar{q}_-)$ line. We adopt the two-cutoff phase space slicing (TCPSS) method [31] to isolate the IR soft singularity. The tree-level Feynman diagrams for this process are shown in Fig.3. In performing the calculations in this work with the TCPSS method, an arbitrary small soft cutoff δ_s should be introduced. The phase space of the $e^+e^- \to q_-\bar{q}_-g$ process can be split into two regions: soft gluon region ($E_5 \leq \frac{1}{2}\delta_s\sqrt{s}$) and hard gluon region ($E_5 > \frac{1}{2}\delta_s\sqrt{s}$) by the soft cutoff δ_s. Thus the cross section for the real gluon emission process is decomposed into soft and hard noncollinear terms, i.e., $\sigma_g^R = \sigma_g^S + \sigma_g^H$. According to the Kinoshita-Lee-Nauenberg (KLN) theorem [32], the soft singularity in the soft part σ_g^S can be canceled by the soft IR divergence in the virtual corrections while the hard cross section part σ_g^H is IR safe.

After eliminating all the UV and IR singularities by performing the renormalization procedure and adding all the QCD NLO correction components, we can get the finite QCD NLO corrected integrated cross section for the $e^+e^- \to q_-\bar{q}_-$ process as

$$\sigma_{NLO} \;\; = \;\; \sigma_{LO} + \Delta\sigma_{NLO} = \sigma_{LO} + \Delta\sigma^{(2)} + \Delta\sigma^{(3)}. \tag{3.8}$$

f (GeV)	$m_{u_-} = m_{c_-}$ (GeV)	$m_{d_-} = m_{s_-}$ (GeV)	$m_{W_H} \approx m_{Z_H}$ (GeV)	m_{A_H} (GeV)
600	830.7	848.5	376.8	82.5
700	974.7	989.9	442.1	99.2
800	1118.0	1131.4	507.1	115.6
900	1260.9	1272.8	571.9	131.8
1000	1403.5	1414.2	636.6	147.8
1100	1545.9	1555.6	701.1	163.7
1200	1688.1	1697.1	765.6	179.5
1300	1830.3	1838.5	830.1	195.2
1400	1972.3	1979.9	894.5	210.9
1500	2114.2	2121.3	958.9	226.6
1600	2256.1	2262.7	1023.2	242.2

Table 2: The masses of T-odd mirror quarks q_- ($q_- = u_-, d_-, c_-, s_-$) and heavy vector boson ($W_H,\ Z_H,\ A_H$) for some typical values of the LHT parameter f taking $\kappa = 1$.

The two-body term $\Delta\sigma^{(2)}$ includes the one-loop corrections to the $e^+e^- \to q_-\bar{q}_-$ process and the tree-level contributions in the soft region for the real gluon emission processes, while the three-body term $\Delta\sigma^{(3)}$ contains the cross sections for the real gluon emission processes over the hard noncollinear region.

IV. Numerical results and discussions

IV..1 Input parameters

The global symmetry breaking scale f is an important parameter of the LHT and has been constrained by recent experiments. Combining all direct LHT new particle searches, an exclusion at 95% CL on the scale f of $f \lesssim 620$ GeV is presented [33]. In our calculations we take the value of f being around this limitation. The CKM matrix is set to be the unit matrix. The other relevant input parameters are chosen as [34] $\alpha_{\rm ew}^{-1} = 137.036$, $m_W = 80.385$ GeV, $m_Z = 91.1876$ GeV, $m_e = 0.511$ MeV. We define $\mu_0 = m_{q_-}$ and fix the T-odd mirror quark mass coefficient κ to be 1 in case no other statement. As a result, the masses of T-odd mirror quarks are only the functions of the LHT parameter f as shown in Eq.(2.1). By using Eq.(2.1) and taking the LHT parameter $\kappa = 1$, we obtain the masses of T-odd mirror quarks for some typical values of the LHT global symmetry breaking scale f listed in Table 2.

IV..2 Checks

The correctness of our calculations are verified through the following aspects:

1. After combining all the contributions at the QCD NLO, the cancelations of UV and IR divergences are verified numerically.

2. We make the verification of the independence of the total NLO QCD correction on δ_s, where an arbitrary cutoff δ_s is introduced to separate the phase space in order to isolate the soft IR divergences [31]. Eq.(3.8) shows that the total NLO QCD corrected cross section (σ_{NLO}) for all the four processes $e^+e^- \to q_\bar{q}_$ ($q_\bar{q}_ = u_\bar{u}_,\ c_\bar{c}_,\ d_\bar{d}_,\ s_\bar{s}_$) is obtained by summing up the two-body and three-body contribution parts ($\sigma_{LO}+\Delta\sigma^{(2)}$ and $\Delta\sigma^{(3)}$). We depict $\sigma_{LO}+\Delta\sigma^{(2)}$, $\Delta\sigma^{(3)}$ and $\sigma_{tot}(=\sigma_{NLO})$ for the $e^+e^- \to q_\bar{q}_$ ($q_\bar{q}_ = u_\bar{u}_,\ c_\bar{c}_,\ d_\bar{d}_,\ s_\bar{s}_$) processes at the $\sqrt{s} = 3$ TeV CLIC as functions of the soft cutoff δ_s in the upper part of Fig.4 with $f = 700$ GeV, $\kappa = 1$ and renormalization scale $\mu = \mu_0 = m_{q_} = 974.7,\ 974.7,\ 989.9,\ 989.9$ GeV for $u_\bar{u}_$-, $c_\bar{c}_$-, $d_\bar{d}_$- and $s_\bar{s}_$-pair production processes, respectively. The amplified curve for the total NLO QCD corrected cross section σ_{tot} in the upper plot of Fig.4, is shown in the lower plot of Fig.4 together with calculation errors. From the figure we can see that the total NLO QCD corrected cross section σ_{NLO} is independent of the cutoff within the statistical errors. That is an indirect check for the correctness of our calculation. In further numerical calculations, we set $\delta_s = 1 \times 10^{-4}$.

IV..3 Dependence on colliding energy $\sqrt{s}$

In the upper part of Fig.5 we present the LO and $\mathcal{O}(\alpha_s)$ QCD corrected cross sections (σ_{LO}, σ_{NLO}) for the $e^+e^- \to q_\bar{q}_$ ($q_\bar{q}_ = u_\bar{u}_,\ c_\bar{c}_,\ d_\bar{d}_,\ s_\bar{s}_$) processes as the functions of colliding energy $\sqrt{s}$ with $f = 1000$ GeV and $\kappa = 1$. The corresponding K-factor defined as $K \equiv \frac{\sigma_{NLO}}{\sigma_{LO}}$, is presented in the lower plot of Fig.5. We can see from Fig.5 that both the LO and NLO QCD corrected cross sections are sensitive to the colliding energy, particularly in the range of $\sqrt{s} \in [2900,\ 3300]$ GeV due to the threshold effect, while decrease quickly when $\sqrt{s} > 3300$ GeV. In the lower plot of Fig.5 it shows that the K-factor has a large value in the vicinity where the colliding energy is close to the $q_\bar{q}_$ threshold due to Coulomb singularity effect.

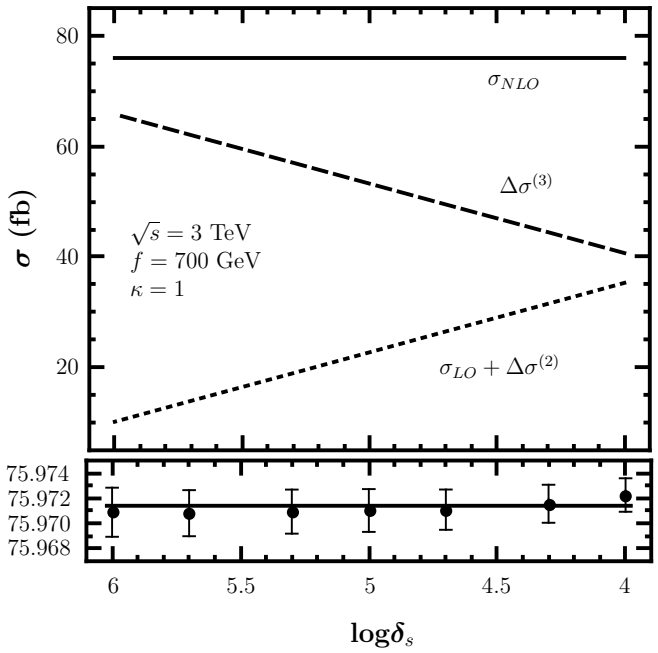

Figure 4: The dependence of the NLO QCD corrected cross section for $e^+e^- \to q_-\bar{q}_-$ ($q_-\bar{q}_- = u_-\bar{u}_-,\ c_-\bar{c}_-,\ d_-\bar{d}_-,\ s_-\bar{s}_-$) on the cutoff δ_s at the $\sqrt{s} = 3$ TeV CLIC, and the amplified curve for $\sigma_{tot}(= \sigma_{NLO})$ with the calculation errors are shown in lower plot.

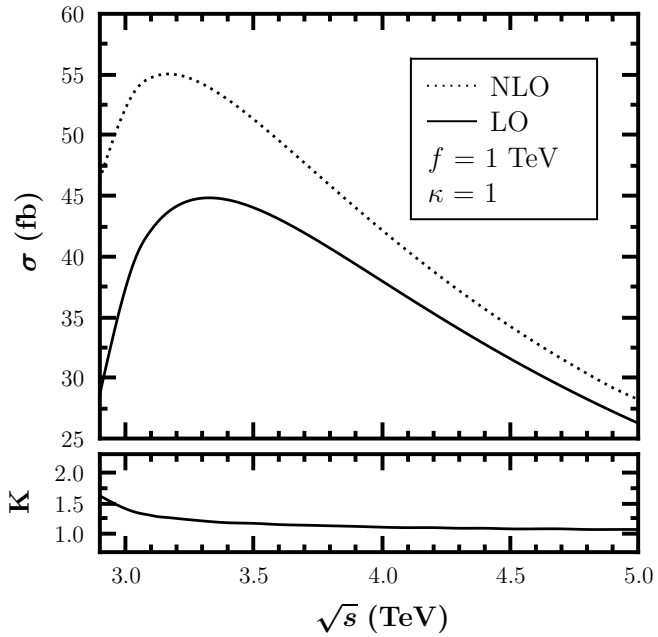

Figure 5: The LO and NLO QCD corrected cross sections for $e^+e^- \to q_-\bar{q}_-$ ($q_-\bar{q}_- = u_-\bar{u}_-,\ c_-\bar{c}_-,\ d_-\bar{d}_-,\ s_-\bar{s}_-$) as functions of colliding energy $\sqrt{s}$ with $f = 1000$ GeV and $\kappa = 1$. The lower plot shows the corresponding K-factor ($K \equiv \frac{\sigma_{NLO}}{\sigma_{LO}}$) as the function of $\sqrt{s}$.

$\sqrt{s}$ (TeV)	f (TeV)	σ_{LO} (fb)	σ_{NLO} (fb)	K
3	700	69.32658(3)	75.9723(5)	1.10
	800	64.19684(3)	72.7819(2)	1.14
	900	55.13894(1)	66.2727(1)	1.20
	1000	37.688101(6)	52.36895(1)	1.39
4	700	41.44320(2)	43.8441(4)	1.06
	1000	37.80775(1)	41.9819(2)	1.11
	1200	30.93860(5)	37.08019(1)	1.20
	1300	24.241070(4)	31.76587(6)	1.31
5	700	26.90824(7)	28.1171(2)	1.05
	900	26.52824(9)	28.0985(3)	1.06
	1000	26.13502(8)	27.9454(1)	1.07
	1100	25.55674(5)	27.65382(8)	1.08
	1300	23.59325(6)	26.42949(9)	1.12
	1500	19.77699(7)	23.64070(9)	1.20
	1600	16.52192(3)	21.06044(4)	1.28

Table 3: The numerical results of σ_{LO}, σ_{NLO} and the corresponding K-factors for the $e^+e^- \to q_-\bar{q}_-$ ($q_-\bar{q}_- = u_-\bar{u}_-,\ c_-\bar{c}_-,\ d_-\bar{d}_-,\ s_-\bar{s}_-$) processes with different values of f and colliding energy $\sqrt{s}$ at the CLIC by taking $\kappa = 1$ and $\mu = \mu_0$.

IV..4 Dependence on global symmetry breaking scale f

We depict the LO, NLO QCD corrected integrated cross sections and the corresponding K-factors as functions of the global symmetry breaking scale f by taking $\kappa = 1$ at the $\sqrt{s} = 3$ TeV, 4 TeV and 5 TeV CLIC in Figs.6(a), (b) and (c), respectively. Figs.6(a,b,c) demonstrate that the LO and NLO QCD corrected total cross sections for the $e^+e^- \to q_-\bar{q}_-$ ($q_-\bar{q}_- = u_-\bar{u}_-,\ c_-\bar{c}_-,\ d_-\bar{d}_-,\ s_-\bar{s}_-$) processes decrease with the increment of f due to the fact that the masses of final q_- and $\bar{q}_-$ become heavier and consequently the phase space becomes smaller as the increment of f. We see that the curves for K-factors in the lower plots of Figs.6(a,b,c) increase slightly with the increament of scale f from 700 GeV to 1000 GeV. The reason is that the threshold value ($2m_{q_-}$) approaches to the colliding energy with the increment of scale f. The numerical results for the $e^+e^- \to q_-\bar{q}_-$ ($q_-\bar{q}_- = u_-\bar{u}_-,\ c_-\bar{c}_-,\ d_-\bar{d}_-,\ s_-\bar{s}_-$) processes at the CLIC for some typical values of f are presented in Table 3.

IV..5 Dependence on T-odd mirror quark mass coefficient κ

In Figs.7(a), (b) and (c) we present the LO, NLO QCD corrected integrated cross sections and the corresponding K-factors as functions of the LHT T-odd quark mass coefficient κ at the $\sqrt{s} = 5$ TeV

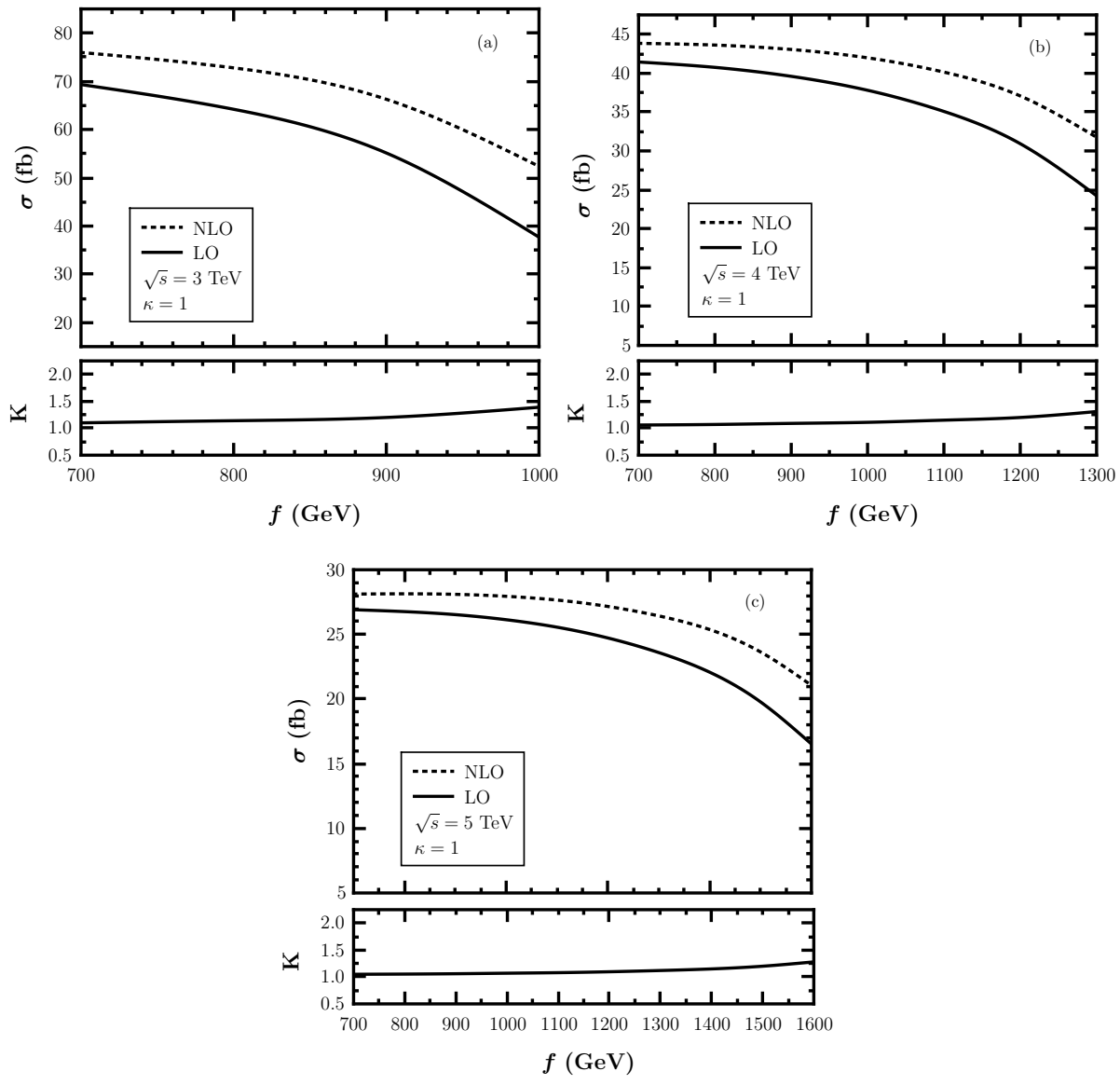

Figure 6: The LO, NLO QCD corrected cross sections and the corresponding K-factor for $e^+e^- \to q_-\bar{q}_-$ ($q_-\bar{q}_- = u_-\bar{u}_-,\ c_-\bar{c}_-,\ d_-\bar{d}_-,\ s_-\bar{s}_-$) as functions of the global symmetry breaking scale f with $\kappa = 1$. (a) $\sqrt{s} = 3$ TeV CLIC. (b) $\sqrt{s} = 4$ TeV CLIC. (c) $\sqrt{s} = 5$ TeV CLIC.

CLIC by taking $\mu_r = \mu_0$ and the global symmetry breaking scale as $f = 1,\ 1.2$ and 1.5 TeV, separately. We can see also from Figs.7(a,b,c) that the NLO QCD correction enhances the integrated cross section, and the LO and NLO QCD corrected total cross sections for $e^+e^- \to q_-\bar{q}_-$ ($q_-\bar{q}_- = u_-\bar{u}_-,\ c_-\bar{c}_-,\ d_-\bar{d}_-,\ s_-\bar{s}_-$) at the $\sqrt{s} = 5$ TeV CLIC decrease with the increment of κ, while the K-factor increases with the increment of κ due to the fact that the threshold value approaches to the colliding energy when κ goes up. We can read from the figures that for $f = 1$ TeV the corresponding K-factor varies from 1.04 to 1.15 with κ going up from 0.6 to 1.4, for $f = 1.2$ TeV the K-factor increases from 1.05 to 1.41 with κ running from 0.6 to 1.4, while for $f = 1.5$ TeV the K-factor goes up from 1.06 to 1.35 with κ increasing from 0.6 to 1.1.

IV..6 Kinematic distributions of final decay products

We are interested in one of the final T-odd mirror quark q_- decay channels, i.e., $q_-(\bar{q}_-) \to A_H q(\bar{q})$. There we get the $q_-(\bar{q}_-)$ decay products involving a $q(\bar{q})$-jet and missing energy of the lightest neutral stable particle A_H. We assume the q_- total decay width being the width summation of the three main decay channels, i.e., $q_- \to V_H q$, ($V_H = Z_H, W_H, A_H$), and the $q_- \to A_H q$ decay branch ratio up to the QCD NLO can be obtained from Eqs.(2.3). We consider the $q_-\bar{q}_-$ pair production process followed by the subsequential decay $q_-(\bar{q}_-) \to A_H q(\bar{q})$ at the CLIC. We plot the LO and NLO QCD corrected distributions of the final $A_H A_H$ pair invariant mass for $e^+e^- \to q_-\bar{q}_- \to 2A_H + 2jets$ ($q_- = u_-, d_-, c_-, s_-$) at the $\sqrt{s} = 3$ TeV CLIC, and the corresponding differential K-factor in Fig.8. The differential K-factor is defined as

$$K(M_{(A_H A_H)}) \equiv \frac{d\sigma_{NLO}/dM_{(A_H A_H)}}{d\sigma_{LO}/dM_{(A_H A_H)}}. \tag{4.1}$$

In this figure we take $f = 700$ GeV and $\kappa = 1$, and get $m_{A_H} = 99.2$ GeV. It demonstrates that the maximal differential cross sections at both the LO and NLO are in the vicinity of $M_{(A_H A_H)} \sim 1.3$ TeV, and the differential K-factor varies from 1.16 to 0.88 when $M_{(A_H A_H)}$ goes up from 300 GeV to 3800 GeV.

For the LO and QCD NLO $e^+e^- \to q_-\bar{q}_- \to 2A_H + 2jets$ events, if the two or three jet (real gluon emission process) event with a jet transverse energies satisfy the condition of $E_{Tj_1} > E_{Tj_2}$ or $E_{Tj_1} > E_{Tj_2} > E_{Tj_3}$, we call j_1 as the leading jet and j_2 as the next-to-leading jet. In Fig.9(a) we

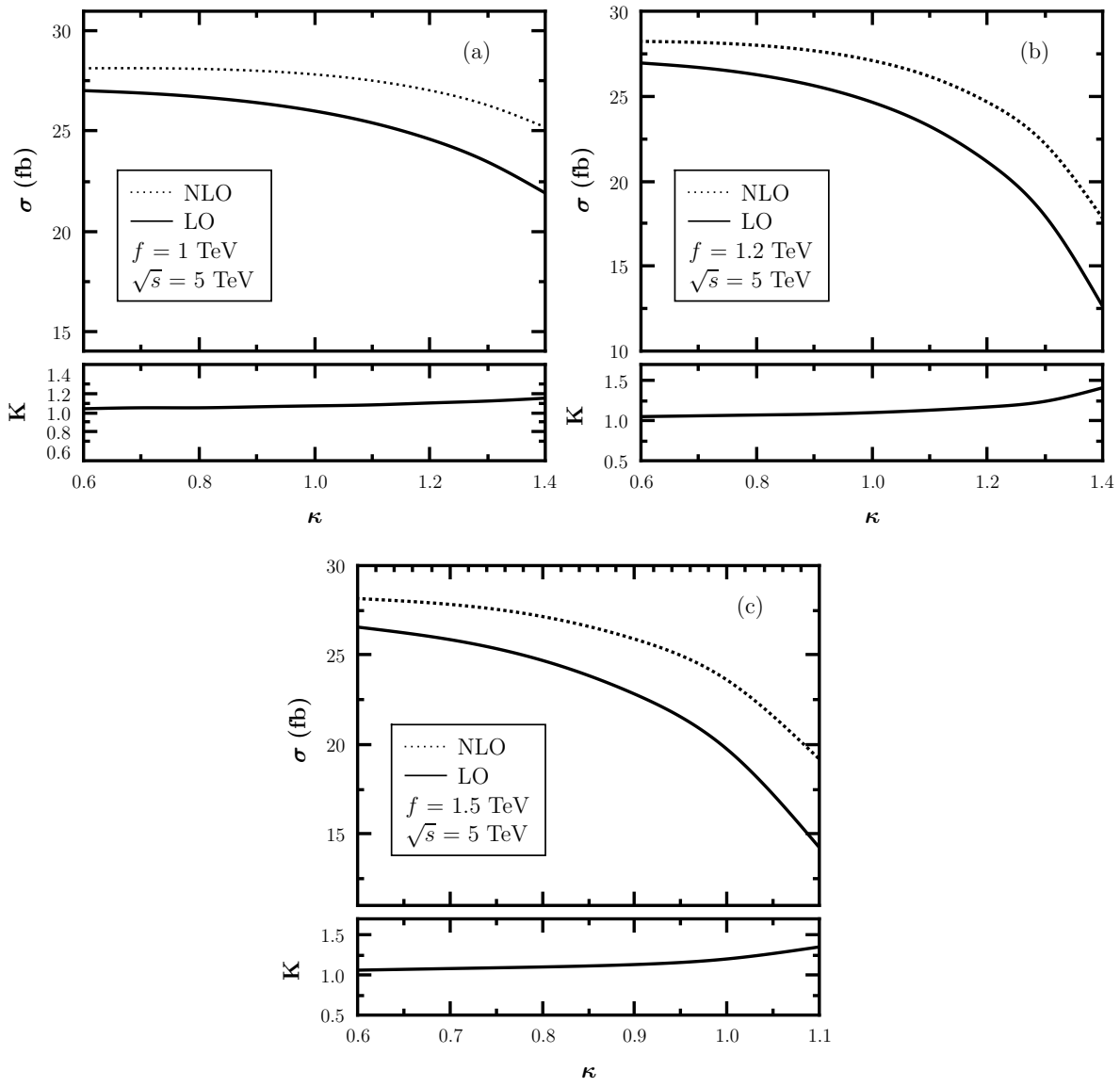

Figure 7: The LO, NLO QCD corrected cross sections and the corresponding K-factors for $e^+e^- \to q_-\bar{q}_-$ ($q_-\bar{q}_- = u_-\bar{u}_-,\ c_-\bar{c}_-,\ d_-\bar{d}_-,\ s_-\bar{s}_-$) as functions of the T-odd mirror quark mass coefficient κ at the $\sqrt{s} = 5$ TeV CLIC. (a) $f = 1$ TeV. (b) $f = 1.2$ TeV. (c) $f = 1.5$ TeV.

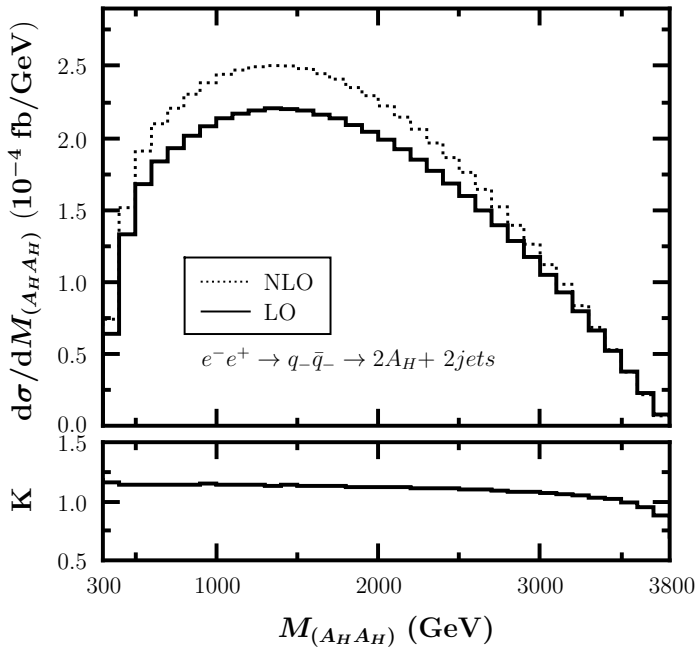

Figure 8: The LO, NLO QCD corrected distributions of the invariant mass of A_HA_H pair, and the corresponding K-factor for $e^+e^- \to q_-\bar{q}_- \to 2A_H + 2jets$ ($q_- = u_-, d_-, c_-, s_-$) at the $\sqrt{s} = 3$ TeV CLIC with $\kappa = 1$ and $f = 700$ GeV.

depict the LO and NLO QCD corrected transverse momentum distributions of the leading jet at the $\sqrt{s} = 3$ TeV CLIC and the corresponding differential K-factor ($K(p_T^{L-jet}) \equiv \frac{d\sigma_{NLO}/dp_T^{L-jet}}{d\sigma_{LO}/dp_T^{L-jet}}$). There we take $f = 700$ GeV and $\kappa = 1$, and get $m_{A_H} = 99.2$ GeV. The figure shows that the NLO QCD correction enhances the LO distribution significantly. We see also that the peaks for the LO and QCD NLO curves are located in the vicinity of $p_T^{L-jet} \sim 1$ TeV, and the differential K-factor runs from 1.08 to 0.88 when p_T^{L-jet} varies from 100 GeV up to 1900 GeV.

In Fig.9(b) the LO and NLO QCD corrected distributions of the rapidity separation of the final leading jet and the next-to-leading jet ($|\Delta y| \equiv |y_{L-jet} - y_{NL-jet}|$), and the corresponding differential K-factor ($K(|\Delta y|) \equiv \frac{d\sigma_{NLO}/d|\Delta y|}{d\sigma_{LO}/d|\Delta y|}$) are plotted. It shows that most of the $e^+e^- \to q_-\bar{q}_- \to 2A_H + 2jets$ events are concentrated in the low $|\Delta y|$ region. We see also that the NLO QCD correction significantly enhances the LO differential cross section, and the differential K-factor varies between 1.13 and 1.31 with $|\Delta y|$ in the range of $[0, 4]$. All the distributions in Fig.8 and Figs.9(a,b) show that a simple approximation of multiplying the LO distribution with the integrated K-factor is not appropriate for precision study of the $e^+e^- \to q_-\bar{q}_-$ ($q_-\bar{q}_- = u_-\bar{u}_-,\ c_-\bar{c}_-,\ d_-\bar{d}_-,\ s_-\bar{s}_-$) processes at the CLIC. It is

necessary to calculate the complete NLO QCD correction to get reliable distributions.

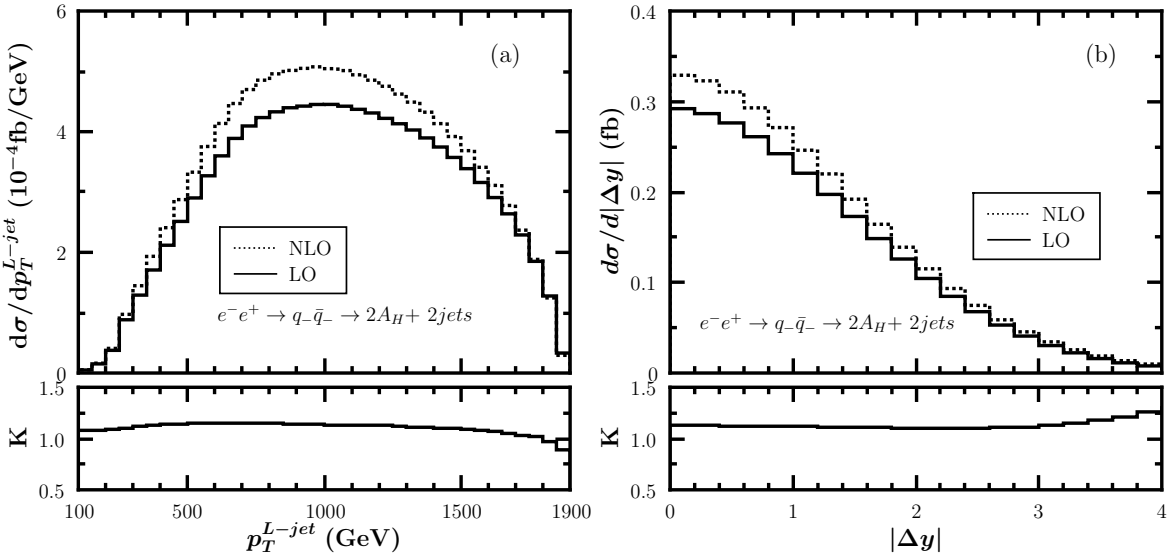

Figure 9: (a) The LO, NLO QCD corrected distributions and the corresponding differential K-factor as functions of the transverse momentum of the leading jet (p_T^{L-jet}) for $e^+e^- \to q_-\bar{q}_- \to 2A_H + 2jets$ ($q_- = u_-,\ c_-, d_-, s_-$) at the $\sqrt{s} = 3$ TeV CLIC with $\kappa = 1$ and $f = 700$ GeV. (b) The LO, NLO QCD corrected distributions and the corresponding K-factor for $e^+e^- \to q_-\bar{q}_- \to 2A_H + 2jets$ ($q_- = u_-,\ c_-, d_-, s_-$) as functions of the rapidity separation of the final leading jet and the next-to-leading jet $|\Delta y| \equiv |y_{L-jet} - y_{NL-jet}|$ at the $\sqrt{s} = 3$ TeV CLIC with $\kappa = 1$ and $f = 700$ GeV.

V. Summary

In this paper we present the precision calculations of the T-odd mirror quark pair production including subsequential weak decays at the e^+e^- CLIC up to the QCD NLO in the littlest Higgs model with T-parity. The future CLIC could provide an efficient facility to put the precision measurements for this production process into practice with a clean environment. The dependence of the NLO QCD effect to the total cross section for the $e^+e^- \to q_-\bar{q}_-$ ($q_-\bar{q}_- = u_-\bar{u}_-,\ c_-\bar{c}_-,\ d_-\bar{d}_-,\ s_-\bar{s}_-$) processes on colliding energy $\sqrt{s}$ is investigated, and the LO and NLO QCD kinematic distributions of final decay products are discussed. We find that the NLO QCD correction always enhances the LO physical observables. The K-factor is clearly related to the observable and the phase space region, and increases obviously when the production threshold approaches the colliding energy. We see that the K-factor for the integrated cross section varies in the ranges of $1.10 \sim 1.39$ ($1.06 \sim 1.31$, $1.05 \sim 1.28$) with $f \in [700,\ 1000]$ GeV ($f \in [700,\ 1300]$ GeV, $f \in [700,\ 1600]$ GeV) at $\sqrt{s} = 3$ TeV (4 TeV, 5 TeV)

CLIC. We conclude that NLO QCD correction has relevant impact on the $e^+e^- \to q_-\bar{q}_- \to 2A_H{+}2jets$ ($q_- = u_-,\ c_-, d_-, s_-$) processes, and should be included in any reliable analysis.

Acknowledgments: This work was supported in part by the National Natural Science Foundation of China (Grants. No.11275190, No.11375008, No.11375171), and the Fundamental Research Funds for the Central Universities (Grant. No.WK2030040044).

References

[1] H. Abramowicz *et al.* 'Physics at the CLIC e^+e^- Linear Collider - Input to the Snowmass process 2013', arXiv:1307.5288.

[2] The European Strategy Group, 'Deliberation Paper on the update of the European Strategy for Particle Physics', May 7, 2013, CERN-Council-S/103/Rev.

[3] CERN Council, 'The European Strategy for Particle Physics - Update 2013, May 7, 2013, CERNCouncil-S/106, 3.

[4] S. Chatrchyan *et al.* [CMS Collaboration], Phys. Lett. **B716**, 30 (2012).

[5] G. Aad *et al.* [ATLAS Collaboration], Phys. Lett. **B716**, 1 (2012).

[6] S. L. Glashow, Nucl. Phys. **22**, 579 (1961).

[7] S. Weinberg, Phys. Rev. Lett. **19**, 1264 (1967).

[8] A. Salam, in Proc. 8th Nobel Symposium Stockholm, 1968, edited by N. Svartholm (Almquist and Wiksells, Stockholm, 1968), p.367.

[9] H. D. Politzer, Phys. Rep. **14**, 129 (1974).

[10] P. W. Higgs, Phys. Lett. **12**, 132 (1964).

[11] Phys. Rev. Lett. **13**, 508 (1964).

[12] P. W. Higgs, Phys. Rev. **145**, 1156 (1966).

[13] F. Englert and R. Brout, Phys. Rev. Lett. **13**, 321 (1964).

[14] G. S. Guralnik, C. R. Hagen and T. W. B. Kibble, Phys. Rev. Lett. **13**, 585 (1964).

[15] T. W. B. Kibble, Phys. Rev. **155**, 1554 (1967).

[16] N. Arkani-Hamed, A.G. Cohen, E. Katz, A.E. Nelson, JHEP **07** (2002) 034.

[17] Hsin-Chia Cheng, Ian Low, JHEP **09** (2003) 051; JHEP **08** (2004) 061.

[18] I. Low, JHEP **10** (2004) 067.

[19] J. Hubisz and P. Meade, Phys. Rev. **D71**, 035016 (2005).

[20] J. Hubisz, P. Meade, A. Noble and M. Perelstein, JHEP **01** (2006) 135.

[21] R. Barbieri and A. Strumia, "The 'LEP paradox'", arXiv:hep-ph/0007265.

[22] H. C. Cheng and I. Low, JHEP **09** (2003) 051; **08** (2004) 061.

[23] R.-Y. Zhang, H. Yan, W.-G. Ma, S.-M. Wang, L. Guo and L. Han, Phys. Rev. **D85**, 015017 (2012).

[24] S.-M. Du, L. Guo, W. Liu, W.-G. Ma and R.-Y. Zhang, Phys. Rev. **D86**, 054027 (2012).

[25] W. Liu, R.-Y. Zhang, L. Guo, W.-G. Ma and L.-W. Chen Phys. Rev. **D87**, 034034 (2013).

[26] A. Belyaev, C.-R. Chen, K. Tobe and C.-P. Yuan, Phys. Rev. **D74**, 115020 (2006).

[27] T. Goto, Y. Okada and Y. Yamamoto, Phys. Lett. **B670**, 378 (2009).

[28] M. Blanke, A. J. Buras, A. Poschenrieder, S. Recksiegel, C. Tarantino, S. Uhlig and A. Weiler JHEP **01** (2007) 066.

[29] T. Hahn, Comput. Phys. Commun. **140**, 418 (2001).

[30] T. Hahn and M. Perez-Victoria, Comput. Phys. Commun. **118**, 153 (1999).

[31] B. W. Harris and J. F. Owens, Phys. Rev. **D65**, 094032 (2002).

[32] T. Kinoshita, J. Math. Phys. (N.Y.) **3**, 650 (1962); T. D. Lee and M. Nauenberg, Phys. Rev. **133**, B1549 (1964).

[33] J. Reuter, M. Tonini and M. de Vries, JHEP **02** (2014) 053.

[34] J. Beringer, *et al.* (Particle Data Group), Phys. Rev. **D86**, 010001 (2012).